11A.1 DIFFERENTIAL REFLECTIVITY BIAS CAUSED BY CROSS COUPLING OF H, V RADIATION FROM THE ANTENNA

Dusan S. Zrnić [*1], Richard J. Doviak[1], Guifu Zhang[2], and Alexander Ryzhkov[3]
[1] National Severe Storms Laboratory, NOAA, Norman OK, 73072
[2] School of Meteorology, University of Oklahoma (OU), Norman OK, 73072
[3] Cooperative Institute for Mesoscale Meteorological Studies, OU, OK 73072

1. INTRODUCTION

The preferred embodiment of dual linear polarization technology on the WSR-88D weather radars is the mode whereby horizontal (H) and vertical (V) polarizations are transmitted and received simultaneously (Doviak et al. 2000). This mode is sometimes referred to as "hybrid" (Wang et al. 2006); to shorten notation we label it SHV (Simultaneous Horizontal and Vertical). The USA National Weather Service is slated to begin retrofitting its WSR-88Ds with this mode in about 2010. By far, the overriding reason for choosing the SHV mode is its total transparency to all the current automated algorithms used in the radar network.

Other advantages of the SHV mode are: 1) direct measurement of the cross correlation between the copolar signals, 2) 360^o unambiguous span for differential phase measurement, 3) decoupling of the differential phase and Doppler velocity measurements, 4) smaller error of estimates, 5) no degradation of the performance of the ground clutter filters, and 6) avoidance of a high power microwave switch and its associated problems. Nonetheless there are also disadvantages. For example, Sachidananda and Zrnic (1985) show, if hydrometeors along a propagation path have a mean canting angle, bias errors in differential reflectivity (Z_{DR}) estimates can be an order of magnitude larger if Z_{DR} estimates are made using the SHV mode rather than alternately transmitting, but simultaneously receiving H, V waves (i.e., the AHV mode). Furthermore, as will be shown, the bias associated with the SHV mode depends on the cross-polar radiation to the first order whereas second order terms are important for the AHV mode. Finally, the SHV mode is not fully polarimetric because it precludes cross-polar measurements.

*Corresponding author address: Dusan S. Zrnić, National Severe Storms Laboratory, Norman, OK 73972; email: Dusan.Zrnic@noaa.gov

The effects of radiation pattern coupling on the measurement accuracies of polarimetric variables were first examined by Chandrasekar and Keeler (1993), but they did not address these accuracies if the SHV mode is used. Because Z_{DR} is a principal variable for estimating rain rate, and because it is more prone to significant bias than other polarimetric variables, we examine Z_{DR} bias caused by coupling of copolar and cross-polar patterns.

Hubbert et al. (2009) have computed the bias caused by cross-polar to copolar pattern coupling assumed to be constant over the significant part of the copolar pattern. Under this assumption they related pattern coupling to the lower limit of linear depolarization ratio measurements. These results, backed by experiment, show Z_{DR} bias (up to 0.27 dB) observed in the SHV mode to be much larger compared to that observed in the AHV mode.

Wang and Chandrasekhar (2006) investigated biases in the polarimetric variables caused by the cross-polar pattern. They have developed pertinent equations building on the formalism in Bringi and Chandrasekar (2001) and quantified biases for a wide range of general conditions. Moreover they present curves for the upper bounds of the errors as function of precipitation type. We examine causes of cross-polar radiation, consider realistic cross-polar patterns, account for differences in the angular dependence of cross-polar and copolar radiation, and reduce the theoretical expressions of Z_{DR} bias to simple compact form. We approximate the principal lobes of the radiation patterns with Gaussian shapes for two common types of cross-polar patterns. Applying these theoretical expressions we obtain the dependence of Z_{DR} bias bounds on copolar and cross-polar pattern parameters and Z_{DR}.

In section 2 we set and justify an upper bound to the Z_{DR} bias based on the accuracy of rain rate measurements, and use that bound to derive limits on the cross-polar radiation pattern. Section 3

quantifies the relation between the cross-polar pattern and bias for practical patterns and includes examples of measured patterns. Section 4 compares the Z_{DR} bias in the SHV and AHV modes.

2. EFFECTS OF Z_{DR} BIAS ON RAIN RATE MEASUREMENTS

Accurate polarimetric measurement has two principal purposes. One is to allow correct classification of precipitation, and the other is to improve quantitative precipitation estimation. In fuzzy logic classification (Zrnic et al. 2001), performance depends on Z_{DR} through the membership (weighting) functions $W_i(Z, Z_{DR}$, etc.). The effects of the Z_{DR} bias on classification can be easily mitigated by appropriately broadening the membership functions. Therefore accurate rainfall measurement imposes a more stringent requirement on the bias of Z_{DR}.

To compute light rain rates (i.e., < 6 mm h^{-1}) the following relation has been proposed for the network of WSR-88Ds (Ryzhkov et al. 2005a),

$$R = \frac{1.70 \times 10^{-2}\, Z_h^{0.714}}{0.4 + 5.0\,|\,Z_{dr} - 1\,|^{1.3}} \quad (\text{mm h}^{-1}), \qquad (1)$$

where Z_h is in units of $mm^6\ m^{-3}$, Z_H(dB) < 36 dBZ, $Z_{dr} = 10^{0.1ZDR}$, and Z_{DR} is in dB. We focus attention to this rain rate regime because it is affected more by Z_{DR} bias. Assuming no error in Z_h, the fractional bias, ΔR/R, in rain rate is,

$$\Delta R/R = f(Z_{DR})/f(Z_{DRb}) - 1\,, \qquad (2a)$$

where

$$f(Z_{DR}) = 0.4 + 5.0\,|\,10^{0.1Z_{DR}} - 1\,|^{1.3}\,, \qquad (2b)$$

and $Z_{DRb} = Z_{DR} + \delta Z_{DR}$ is the biased differential reflectivity. It follows from (2) that the fractional error is slightly larger if the dB bias in differential reflectivity is negative. Hence the fractional biases in R are plotted (Fig. 1) for three negative values of Z_{DR} bias.

Implications of bias can be assessed by comparing the polarimetric estimates of R with that obtain using a commonly accepted $R(Z)$ relation. For such a stand-alone relation (i.e., no adjustment with gage data) the rms errors are about 35 % (Brandes et al. 2002, Balakrishnan et al. 1989, Ryzhkov and Zrnic 1995). But, with judicious use of polarimetric data, R errors could be reduced to between 15 and 22 % (Zhang et al. 2001; Ryzhkov et al. 2005b; Matrosov et al. 2002). Thus it is reasonable to strive to keep $\Delta R / R$ less than about 20 % implying that the absolute bias in differential reflectivity should be less than 0.15 dB.

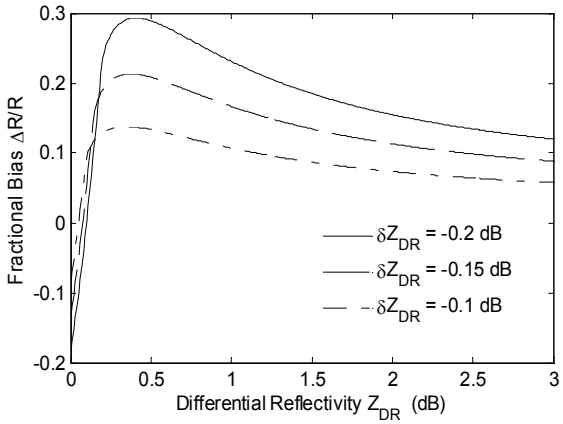

Fig. 1 Fractional bias, $\Delta R / R$, of rain rate R vs differential reflectivity Z_{DR}, with bias δZ_{DR} as a parameter.

Two independent mechanisms produce Z_{DR} bias: 1) a small but constant offset due to calibration error (this can be kept within ±0.1 dB; Zrnic et al. 2006), and 2) the presence of cross-polar radiation. Bias, δZ_{DR}, depends (as shown later) on Z_{DR}, β (i.e., the phase difference between the transmitted H, V copolar radiation), γ the phase difference between the copolar and cross-polar radiation, and the total differential phase change Φ_{DP} along the propagation path.

3. RADIATION PATTERN COUPLING FOR THE SHV MODE

3.1. *An expression for the bias*

Consider a circularly symmetric parabolic reflector antenna and uniform distribution of scatterers. Performance characteristics of such antennas for dual polarization radars are discussed by Bringi and Chandrasekar (2001, section 6.2). These authors provide error budget and integral formulas for biases applicable to the AHV mode. With similar simplification, but extending the analysis to cross-polar patterns that are different than the copolar pattern, we formulate equations for the Z_{DR} bias incurred with the SHV and AHV modes.

The effects on Z_{DR} will be quantified under the following conditions. The intrinsic Z_{DR} is produced

by oblate scatterers having zero canting angles so that the off -diagonal terms of the backscattering matrix are zero. The amplitudes of the transmitted electric fields in the H and V channels are assumed to be matched, but there is a differential phase β between the two at the feed horn aperture. Differential attenuation along the path of propagation can, for most observations at 10 cm wavelengths, be neglected, but Φ_{DP} cannot be ignored. To simplify notation, Φ_{DP} is incorporated into the backscattering matrix $\mathbf{S}$ observed at the radar (i.e., Φ_{DP} is merged with the scatterer's backscatter differential phase). Furthermore, it is not necessary to include the resolution volume depth; thus the function F (Doviak and Zrnic, 2006; section 8.5.2.2), weighting the polarimetric properties of a scatterer, is only proportional to the intensity and phase of the radiation pattern at angles θ, φ.

With these conditions we write the matrix equation for the SHV mode

$$\begin{vmatrix} \delta V_h \\ \delta V_v \end{vmatrix} \equiv \vec{V} = \mathbf{F}^t \mathbf{S} \mathbf{F} \vec{E}_i = \begin{vmatrix} F_{hh} & F_{vh} \\ F_{hv} & F_{vv} \end{vmatrix} \begin{vmatrix} s_{hh} & 0 \\ 0 & s_{vv} \end{vmatrix} \begin{vmatrix} F_{hh} & F_{hv} \\ F_{vh} & F_{vv} \end{vmatrix} \begin{vmatrix} 1 \\ e^{j\beta} \end{vmatrix} \quad (3)$$

for the received H and V channel incremental voltages generated by a scatterer. (In case of the AHV mode we would write $\delta V_h = \delta V_{hi}$, and $\delta V_v = \delta V_{vi}$ where 'i' is either h or v, the first index identifying the H or V channel receiving the signal, and the second index identifying the transmitting channel, and the $\vec{E}_i$ vector's polarization would alternate between H and V every PRT). The superscript "t" denotes the transpose matrix, $\vec{E}_i$ is the transmitted electric field in the feed horn aperture. F_{hv} is proportional to the H radiated electric field if the V channel is excited, and vice versa for F_{vh}. Constants of proportionality, that would make this equation dimensionally correct, and the arguments of F_{ij} and s_{ij} (i, j are either h or v), are not shown to shorten the notation; these omissions have no effect whatsoever on our results. The pattern functions F_{ij} are not normalized but contain the peak power gain g_{ij} so that

$$F_{ij}(\theta,\phi) = \sqrt{g_{ij}} f_{ij}(\theta,\phi). \quad (4)$$

The spherical angles (θ,ϕ) are relative to the copolar beam axis.

It is further stipulated that $F_{hh} = F_{vv}$ is a real function (i.e., has zero reference phase), but F_{hv}, F_{vh} are complex (i.e., F_{hv} and F_{vh} have phases γ_{hv} and γ_{vh} relative to the copolar phase).

Executing the matrix multiplication in (3) the following equation ensues

$$\begin{vmatrix} \delta V_h \\ \delta V_v \end{vmatrix} = \begin{vmatrix} s_{hh}F_{hh}(F_{hh} + F_{hv}e^{j\beta}) + s_{vv}F_{vh}(F_{vh} + F_{hh}e^{j\beta}) \\ s_{hh}F_{hv}(F_{hh} + F_{hv}e^{j\beta}) + s_{vv}F_{hh}(F_{vh} + F_{hh}e^{j\beta}) \end{vmatrix}. \quad (5)$$

Of interest are the powers from the ensemble of scatterers weighted by pattern functions.

Thus we will take the ensemble average $<|\delta V_h|^2>$ and integrate it over the pattern functions to obtain the power received in the H channel

$$P_h \sim \iint_{\theta,\phi} <|\delta V_h|^2> \sin\theta d\theta d\phi = \int_\Omega \left\{ \begin{matrix} <|s_{hh}F_{hh}(F_{hh} + F_{hv}e^{j\beta}) + \\ s_{vv}F_{vh}(F_{vh} + F_{hh}e^{j\beta})|^2> \end{matrix} \right\} d\Omega, \quad (6)$$

where < > indicates ensemble average over the distribution of the scatterers' properties (Doviak and Zrnic 2006; Eq.8.45). To shorten notation, $\sin\theta d\theta d\phi$ is replaced with $d\Omega$. A very similar expression for P_v follows from the second row of (5).

The integral in (6) can be expressed as the sum of three terms of which the first (containing s_{hh}) is

$$\int_\Omega <|s_{hh}F_{hh}(F_{hh} + F_{hv}e^{j\beta})|^2> d\Omega = <|s_{hh}|^2> \int_\Omega \left\{ F_{hh}^2 \begin{bmatrix} F_{hh}^2 + 2F_{hh}\,\mathrm{Re}(F_{hv}e^{j\beta}) \\ +|F_{hv}|^2 \end{bmatrix} \right\} d\Omega, \quad (7a)$$

where it is assumed that the ensemble averages of the backscattering second moments (e.g., $<|s_{hh}|^2>$) are constant in regions where the pattern functions are significant.

The second term is the cross product involving s_{hh} and s_{vv}, and is given by

$$2\int_{\Omega}\left\{\mathrm{Re}\left[\begin{array}{l}<s_{hh}s_{vv}^{*}> \\ \left(F_{hh}^{2}F_{vh}^{*2}+F_{hh}F_{hv}F_{vh}^{*2}e^{j\beta}+\right. \\ \left.F_{hh}{}^{3}F_{vh}^{*}e^{-j\beta}+F_{hh}^{2}F_{hv}F_{vh}^{*}\right)\end{array}\right]\right\}d\Omega \quad (7b)$$

and the third term, the magnitude squared of the second term in (6), is

$$\int_{\Omega}<|s_{vv}F_{vh}(F_{vh}+F_{hh}e^{j\beta})|^{2}>d\Omega =$$

$$<|s_{vv}|^{2}>\int_{\Omega}\left\{|F_{vh}|^{2}\left[\begin{array}{l}|F_{vh}|^{2}+ \\ 2F_{hh}\,\mathrm{Re}(F_{vh}e^{-j\beta})+ \\ F_{hh}{}^{2}\end{array}\right]\right\}d\Omega \quad (7c)$$

Next are listed the corresponding three terms comprising the vertically polarized power:

$$<|s_{hh}|^{2}>\int_{\Omega}|F_{hv}|^{2}\left[\begin{array}{l}F_{hh}^{2}+ \\ 2F_{hh}\,\mathrm{Re}(F_{hv}e^{j\beta}) \\ +|F_{hv}|^{2}\end{array}\right]d\Omega \quad (8a)$$

$$2\int_{\Omega}\mathrm{Re}\left[\begin{array}{l}<s_{hh}s_{vv}^{*}>(F_{hv}^{2}F_{hh}^{2}+ \\ F_{hh}F_{vh}^{*}F_{hv}^{2}e^{j\beta}+F_{hv}F_{hh}^{3}e^{-j\beta} \\ +F_{hh}^{2}F_{hv}F_{vh}^{*})\end{array}\right]d\Omega, \quad (8b)$$

and

$$<|s_{vv}|^{2}>\int_{\Omega}F_{hh}^{2}\left[\begin{array}{l}|F_{vh}|^{2}+ \\ 2F_{hh}\,\mathrm{Re}(F_{vh}e^{-j\beta})+F_{hh}^{2}\end{array}\right]d\Omega. \quad (8c)$$

The bias δZ_{DR} expressed in dB is computed from

$$\delta Z_{DR}=10\log(P_{h}/P_{v})-Z_{DR}, \quad (9)$$

for specific values of the system parameters and polarimetric variables. In the sequel the differential reflectivity in linear units, that is

$$Z_{dr}=\frac{<|s_{hh}|^{2}>}{<|s_{vv}|^{2}>}, \quad (10a)$$

as well as the copolar correlation coefficient

$$\rho_{hv}e^{j\Phi_{DP}}=\frac{<s_{hh}^{*}s_{vv}>}{\sqrt{<|s_{hh}|^{2}><|s_{vv}|^{2}>}}, \quad (10b)$$

will be used.

The expressions for computing bias are applicable to arbitrary copolar and cross-polar patterns. Center fed parabolic reflectors are designed to have very low cross-polar radiation. Thus one can drop the third and fourth order terms in F_{hv} and F_{vh}, sum the remaining terms in (7) and (8), and divide the powers P_h and P_v with $<|s_{vv}|^2>$ to obtain

$$\frac{P_{h}}{<|s_{vv}|^{2}>}=$$

$$Z_{dr}\int_{\Omega}\left\{\begin{array}{l}F_{hh}^{2}\left[\begin{array}{l}F_{hh}^{2}+2F_{hh}\,\mathrm{Re}(F_{hv}e^{j\beta}) \\ +|F_{hv}|^{2}\end{array}\right]+ \\ 2\rho_{hv}\dfrac{F_{hh}^{2}}{Z_{dr}^{1/2}}\mathrm{Re}\left[\begin{array}{l}e^{-j\Phi_{DP}}(F_{vh}^{*2}+ \\ F_{hh}F_{vh}^{*}e^{-j\beta}+ \\ F_{hv}F_{vh}^{*})\end{array}\right] \\ +Z_{dr}^{-1}F_{hh}^{2}|F_{vh}|^{2}\end{array}\right\}d\Omega \quad (11a)$$

and

$$\frac{P_{v}}{<|s_{vv}|^{2}>}=$$

$$\int_{\Omega}\left\{\begin{array}{l}2\rho_{hv}Z_{dr}^{1/2}F_{hh}^{2}\,\mathrm{Re}\left[\begin{array}{l}e^{-j\Phi_{DP}}(F_{hv}^{2}+ \\ F_{hh}F_{hv}e^{-j\beta}+ \\ F_{hv}F_{vh}^{*})\end{array}\right]+ \\ Z_{dr}F_{hh}^{2}|F_{hv}|^{2}+F_{hh}^{2}\left[\begin{array}{l}|F_{vh}|^{2}+ \\ 2F_{hh}\,\mathrm{Re}(F_{vh}e^{-j\beta}) \\ +F_{hh}^{2}\end{array}\right]\end{array}\right\}d\Omega \quad (11b)$$

The decibel of biased differential reflectivity is the difference in the decibel logarithms of (11a) and (11b). Note $\int_{\Omega} F_{\rm hh}^4 d\Omega$ is much larger than any of the other terms in (11a and b). Dividing these two equations with this term and taking the difference of logarithmic functions produces the bias. Because the arguments of the logarithmic functions are close to 1, we use the first order Taylor expansion and express the bias as

$$\delta Z_{\rm DR} = 10(A_1 + A_2)\log e \qquad (12a)$$

where the term A_1 contains integrals of F_{hv} to first order and A_2 contains the integrals of F_{hv} to second order. Explicitly

$$A_1 = \frac{2\int F_{\rm hh}^3 \,{\rm Re}\left\{ \begin{array}{l} F_{\rm hv} e^{j\beta} - F_{\rm vh} e^{-j\beta} + \rho_{\rm hv} \times \\ \left[e^{-j\Phi_{\rm DP}} \left(\begin{array}{l} Z_{\rm dr}^{-1/2} F_{\rm vh}^* e^{-j\beta} - \\ Z_{\rm dr}^{1/2} F_{\rm hv} e^{-j\beta} \end{array} \right) \right] \end{array} \right\} d\Omega}{\int F_{\rm hh}^4 d\Omega} \qquad (12b)$$

$$A_2 = \frac{\int F_{\rm hh}^2 \left\{ \begin{array}{l} |F_{\rm hv}|^2 - |F_{\rm vh}|^2 + Z_{\rm dr}^{-1} |F_{\rm vh}|^2 \\ -Z_{\rm dr} |F_{\rm hv}|^2 + 2\rho_{\rm hv} \times \\ {\rm Re}\left\{ \begin{array}{l} e^{-j\Phi_{\rm DP}} [Z_{\rm dr}^{-1/2} (F_{\rm vh}^{*2} + \\ F_{\rm hv} F_{\rm vh}^*) - \\ Z_{\rm dr}^{1/2} (F_{\rm hv}^2 + F_{\rm hv} F_{\rm vh}^*)] \end{array} \right\} \end{array} \right\} d\Omega}{\int_{\Omega} F_{\rm hh}^4 d\Omega} \qquad (12c)$$

3.2 *Types of cross-polar radiation patterns*

In the literature one finds cross-polar pattern types to which the expressions developed herein are applicable. One type has a prominent cross-polar lobe coaxial with the copolar beam. This pattern is discussed in the next section. A second type has a quad of principal cross-polar lobes located diagonally to the H and E principal planes; this is typical of a center feed parabolic reflector (Fradin 1961). For parabolic reflectors with offset feeds, the number of principal cross-polar lobes is reduced to two (Durić et al. 2008). Finally there are cross-polar patterns that appear to be a combination of the first two types. Contours of the main lobes for these pattern types are sketched in Fig. 2.

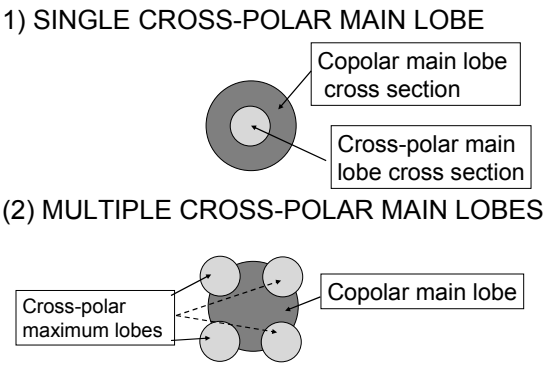

Fig. 2 Cross sections through the copolar main lobe and cross-polar main lobes for two types of cross-polar patterns: (1) A single cross-polar lobe centered on the beam axis of the copolar main lobe, (2) Four equal cross-polar lobes superposed on the copolar main lobe skirts.

Prior to quantifying the bias, a brief discussion of radiation patterns follows starting with the one measured for the KOUN radar. This pattern is examined for obvious practical reasons, which are to quantify its effects on the KOUN polarimetric radar and to anticipate the performance of the forthcoming dual-polarization WSR-88D radars. Measurements of the H cross-polar radiation field indicate a cross-polar pattern with a peak about 30 dB below the V copolar peak, centered on the copolar beam axis. We have also examined cross-polar patterns measured by Andrew Canada (Paramax 1992) on another WSR-88D reflector illuminated with a feed that generates a single linear polarized field (i.e., horizontal). The measurement shows a cross-polar main lobe coaxial with the copolar lobe, and the ratio of the cross-polar peak to copolar peak is about the same as that measured for the KOUN. Although the WSR-88D antennas have cross-polar patterns that are likely a combination of the two types shown in Fig.2, cross-polar peaks coaxial with the copolar beam appear are the most significant contributor to $Z_{\rm DR}$ bias; thus we will first focus on that pattern.

The principal contributor to the coaxial cross-polar peak is thought to be the cross-polar pattern of the feed horn illuminating the reflector (Doviak and Zrnic 1998). The cause of cross-polar peaks along the beam axis of the feed has not been established, but it is known that concentricity and circularity of the horn components on the order of a few thousandths of a wavelength are necessary to substantially reduce spurious emissions (Potter 1963). For a well-designed and fabricated polarimetric feed horn, and an ideal parabolic reflector, the cross-polar radiation should vanish along the principal planes; thus there should be a null on-axis. In this case the only prominent peaks of cross-polar radiation should be that associated with the reflector (Appendix).

Cross-polar pattern measurements on large antennas are more difficult to make and interpret than copolar patterns because cross-polar radiation is weak and the copolar radiation incident on the terrain surrounding the radar site can be converted to cross-polar radiation upon scatter (Doviak and Zrnic 1998, section II.6.3). This is worse at low elevation angles where parts of the copolar beam could illuminate the foreground. Thus the lack of a well defined on-axis null could be an artifact of the site where patterns are measured.

Although there can be many causes of the coaxial cross-polar peak radiation, we shall focus our formulation on two specific ones, and for each of these we shall specify the amplitude and phase of F_{hv} and F_{vh}. Cross-polar radiation (i.e., H radiation fields if the V antenna port is excited and vice versa) can be generated by: 1) a rotation of the horn about its axis (Doviak and Zrnic 1998), and 2) a lack of geometric orthogonality of the H and V ports. There might be other causes, and for comparisons we also examine the worst possible case. Next we develop expressions for Z_{DR} bias in case of coincident copolar and cross-polar pattern peaks.

3.3 Z_{DR} bias due to coaxial copolar and cross-polar pattern lobes

The first order F_{hv}, F_{vh} terms in A_1 (12b) are much larger than the second order terms in A_2 (12c); hence A_2 can be ignored so that the bias (12a) can be written as

$$\delta Z_{DR} = 20\log(e)\left\{\begin{array}{l} W_{hv}\left[\begin{array}{l}\cos(\beta+\gamma_{hv})- \\ \rho_{hv}Z_{dr}^{1/2}\cos(\Phi_{DP}+\beta-\gamma_{hv})\end{array}\right] \\ -W_{vh}\left[\begin{array}{l}\cos(\beta-\gamma_{vh})- \\ \dfrac{\rho_{hv}}{Z_{dr}^{1/2}}\cos(\Phi_{DP}+\beta+\gamma_{vh})\end{array}\right]\end{array}\right\} \quad (13)$$

where γ_{hv} and γ_{vh} are the phases of the cross-polar radiation relative to the copolar phase,

$$W_{hv} = \int F_{hh}^3 \,|F_{hv}|d\Omega \,/ \int F_{hh}^4 d\Omega \ , \qquad (14a)$$

and

$$W_{vh} = \int F_{hh}^3 \,|F_{vh}|d\Omega \,/ \int F_{hh}^4 d\Omega \ , \qquad (14b)$$

are the antenna's bias weighting factors that measure the effectiveness of the integrated product of copolar and cross-polar fields in generating Z_{DR} bias. These weighting factors can be conservatively specified so that the bias is always smaller than a prescribed value. This conservative specification can be relaxed, as demonstrated next, if the various phases are appropriately adjusted.

Let's first consider the case $F_{hv} = F_{vh}$. Thus, defining $W_{hv} = W_{vh} = W$ and $\gamma_{hv} = \gamma_{vh} = \gamma$ and substituting these into (13) produces

$$\delta Z_{DR} \approx 20\log(e)W\left\{\begin{array}{l}-2\sin(\beta)\sin(\gamma)+ \\ \rho_{hv}\left[\begin{array}{l}Z_{dr}^{-1/2}\cos(\Phi_{DP}+\beta+\gamma) \\ -Z_{dr}^{1/2}\cos(\Phi_{DP}+\beta-\gamma)\end{array}\right]\end{array}\right\} \text{ (dB). (15)}$$

This equation indicates that the maximum bounds on δZ_{DR} are

$$\delta Z_{DR} \approx \pm 20\log(e)W\left\{2+\rho_{hv}\left[Z_{dr}^{-1/2}+Z_{dr}^{1/2}\right]\right\} \ . (16a)$$

These bounds occur if $\beta = \pm 90^o$, $\gamma = \mp 90^o$, and $\Phi_{DP} = 0$ (i.e., bias is always positive) or $\gamma = \pm 90^o$ and $\Phi_{DP} = 180^o$ (i.e., bias is always negative). Thus depending on the particular values of the phases (β, γ, and Φ_{DP}) the bias can take any value between the boundaries given by (16a).

Because for rain $\left[Z_{\rm dr}^{-1/2} + Z_{\rm dr}^{1/2} \right] \approx 2$, and $\rho_{\rm hv} \approx 1$, the largest positive or negative bias is

$$\delta Z_{\rm DR} \approx \pm 80 W \log(e) = \pm 35 W \text{ (dB)}. \quad (16b)$$

These large biases can be incurred if the transmitted wave is circularly polarized, and the cross-polar and copolar fields are in phase quadrature.

From (15) it can be deduced that the narrowest span of bias occurs if β = 0° or 180°, and γ = 180° or 0°. Then the bias is contained within the maximum bounds (i.e., for $\Phi_{\rm DP}$ = $0, \pi$)

$$\delta Z_{\rm DR} \approx \pm 20 W \log(e) \rho_{\rm hv} (Z_{\rm dr}^{1/2} - Z_{\rm dr}^{-1/2}) \quad (16c)$$

To achieve this narrow span of bias, the transmitted field should be slanted linear at either $\pm 45^{\rm o}$ while the cross-polar field within the main lobe should be in or out of phase with respect to the phase of the copolar field. Control of the transmitted phase β is practical, but the phase difference between cross-polar and copolar main fields is typically the intrinsic property of the antenna, and perhaps of its site.

Suppose that the phase difference β is set to 0° or 180° (by design), but the cross-polar field is in phase quadrature with the copolar field (i.e., $\gamma = \pm 90^{\rm o}$). Under these conditions, $\delta Z_{\rm DR}$ is now contained within the intermediate bounds

$$\delta Z_{\rm DR} \approx \pm 20 W \log(e) \rho_{\rm hv} (Z_{\rm dr}^{-1/2} + Z_{\rm dr}^{1/2}) \approx \pm 17.4 W . \quad (16d)$$

These three bias boundaries (i.e., 16b, 16c, and 16d), with $\delta Z_{\rm DR}$ normalized by W), are plotted versus $Z_{\rm DR}$, in Fig.3.

In summary, Fig. 3 indicates that the upper boundary of bias (top curve) is incurred if $\beta = \pm 90^{\rm o}$ (i.e., circularly polarized transmitted field) and $\gamma = 90^{\rm o}$. Change in any one of these would therefore reduce the bias boundaries. With β adjusted to minimize the bias (e.g., $\beta = 0^{\rm o}$) the worst case of positive bias is the middle curve (16d). This middle boundary and the highest one are essentially independent of $Z_{\rm DR}$. For the case $\beta = 0^{\rm o}$ and $\gamma = 180^{\rm o}$ the maximum positive bias is the lowest curve. In the region of $Z_{\rm DR}$ typical for rain, the boundaries are practically linear functions of $Z_{\rm DR}$.

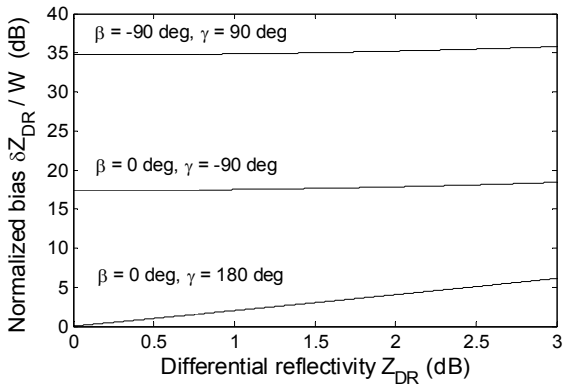

Fig. 3 Envelopes of the maximum positive $Z_{\rm DR}$ bias normalized by W (linear scale), for $\rho_{\rm hv}$=1, and the indicated values of the phases. Envelopes of the maximum negative bias are mirror images of these curves with respect to the abscissa.

We shall use Fig. 3 to determine the bias for some possible values of the antenna gains. Assume axially symmetric Gaussian radiation patterns so that $\left| f_{\rm ij}(\theta) \right|^2 = \exp[-\theta^2 / (4\sigma_{\rm ij}^2)]$ describes the one-way power pattern (Doviak and Zrnic 2006; section 5.3). Then

$$W_{hv} = \frac{4\theta_{\rm 1x}^2}{\theta_{\rm 1}^2 + 3\theta_{\rm 1x}^2} \cdot \frac{g_{\rm hv}^{1/2}}{g_{\rm hh}^{1/2}} \quad (17a)$$

and

$$W_{\rm vh} = \frac{4\theta_{\rm 1x}^2}{\theta_{\rm 1}^2 + 3\theta_{\rm 1x}^2} \cdot \frac{g_{\rm vh}^{1/2}}{g_{\rm hh}^{1/2}}, \quad 17b)$$

where the one-way 3 dB beamwidths of the copolar and cross-polar power patterns are θ_1 and θ_{1x}. For equal beamwidths and if the peak of the cross polar pattern is 40 dB below the copolar peak, W = 0.01. From Fig. 3 we find that the maximum positive bias is about 0.35 dB (i.e., for $\Phi_{\rm DP}$ = 0). This bias would drop to about 0.18 dB if $\pm 45^{\rm o}$ slant linearly polarized waves are transmitted; this would produce a maximum rain rate error of less than 25% (Fig. 1). Further reduction is possible only if the copolar and cross-polar patterns are in phase (or 180° out of phase). Nevertheless, as the electromagnetic wave propagates into the rain filled medium the bias and fractional rain rate errors will decrease.

3.3.1 $Z_{\rm DR}$ BIAS DUE TO A ROTATED HORN

It will be assumed that rotation of the horn in the polarization plane is the only mechanism causing cross-coupling. That is, the cross-polar radiation with a properly oriented horn is negligible (i.e., the intrinsic $F_{hv} = F_{vh} = 0$). Computing the bias in this case can be done by introducing the rotation matrix in equation (3). Multiplying the rotation matrix with the F matrix we obtain the effective matrix $\mathbf{F}^{(e)}$

$$\mathbf{F}^{(e)} = \begin{vmatrix} F_{hh}\cos\alpha & -F_{hh}\sin\alpha \\ F_{hh}\sin\alpha & F_{hh}\cos\alpha \end{vmatrix}, \qquad (18)$$

where α is the rotation angle with a positive sign counter-clockwise. In this case $F_{hv}^{(e)} = -F_{hh}\sin\alpha$, $F_{vh}^{(e)} = F_{hh}\sin\alpha$, etc. Then introducing the terms from (18) into (3) and carrying forward the computations, the following approximate formula for the bias is obtained:

$$\delta Z_{DR} \approx 20W\log(e)\begin{bmatrix} -2\cos(\beta) + \\ \rho_{hv}(Z_{dr}^{-1/2} + Z_{dr}^{1/2})\cos(\Phi_{DP} + \beta) \end{bmatrix} \qquad (19)$$

where now the bias weighting factor $W = \tan(\alpha)$. For small angular rotations, this result agrees with that obtained by Doviak et al. (2000).

Feed horn rotation can be set to tolerances of the order of 0.1^o (Doviak and Zrnic 1998, section II.6.7) at which level $\tan(0.1^o) = 0.0017$, and the maximum bias (top curve in Fig. 3) is about 0.06 dB. Hence for practically designed antennas, horn rotation should not be a factor.

3.3.2 BIAS DUE TO NONORTHOGONALITY OF THE H AND V PORTS

Let's assume that the H, V ports are separated by an angle $\chi < \pi/2$ and the horn is rotated about its axis to null one of the cross-polar fields. For example, if the cross-polar V field produced by excitation of the H port had an on-axis null (i.e., $F_{vh} = 0$), the copolar H field would be F_{hh}. But if the V port is then excited, the cross-polar H would be $-F_{hh}\sin\alpha$, where $\alpha = (\pi/2) - \chi$ (α positive counter-clockwise), and the copolar V would be $F_{hh}\cos\alpha$. Thus the matrix $\mathbf{F}^{(e)}$ becomes

$$\mathbf{F}^{(e)} = \begin{vmatrix} F_{hh} & -F_{hh}\sin\alpha \\ 0 & F_{hh}\cos\alpha \end{vmatrix}, \qquad (20)$$

and by substituting the terms from (20) into (3) and simplifying, the following bias equation is obtained,

$$\delta Z_{DR} \approx 20W_1\log(e)\left[-\cos(\beta) + \rho_{hv}Z_{dr}^{1/2}\cos(\Phi_{DP} + \beta)\right] \qquad (21)$$

In (21) $W_1 = \sin\alpha$ and, as with (19), the bias peaks at $\beta = -90^o$ and $\Phi_{DP} = 90^o$. At the same α tolerance as that for the rotated horn, bias is insignificant.

3.4 *Z_{DR} bias due to a four-lobed cross-polar radiation pattern*

Cross-polar radiation patterns with nulls along the principal planes and a distinct equal amplitude principal peak near the copolar peak in each of the quadrants (Fig. 3b) is the subject of this section. This type pattern is inherent to a center-fed parabolic reflector illuminated with linearly polarized radiation (Fradin 1961, section VII.2). For an example the reader is referred to Chandrasekar and Keeler (1993, Fig. 11). Offset parabolic reflectors (e.g., the SPIRA polarimetric imaging radiometer, Durić et al. 2008) produce cross-polar patterns with two principal peaks near the copolar peak. These cross-polarized peaks, inherent to the parabolic reflector, can be substantially reduced if a circular horn is used to illuminate the reflector (Fradin 1961, VII.3). The general procedure used in section 3*a* to compute Z_{DR} biases also applies to this case. Nonetheless, to obtain analytical solutions, further simplification and assumptions are required.

The electric field pattern $f_{h\,v}(\theta,\phi)$ is assumed to be axially symmetric about its peak, but the electric field at each peak alternates in sign as one passes from one peak to the next around the copolar beam axis; thus the copolar and cross-polar fields are in phase or anti-phase, and $|F_{hv}| = |F_{vh}|$ (Appendix). Therefore the terms $F_{hh}^k F_{hv}^n$ in (7) integrate to zero for any k if the exponent n is odd and if there is an even number of peaks; that is, the first order and third order terms in F_{hv} vanish. Hence $A_1 = 0$ so that A_2 from (12c) produces the bias

$$\delta Z_{\mathrm{DR}} = -10\log(e)\frac{\int F_{\mathrm{hh}}^2 \,|F_{\mathrm{hv}}|^2 \, d\Omega}{\int F_{\mathrm{hh}}^4 d\Omega} \times \left[\begin{array}{l} Z_{\mathrm{dr}} - Z_{\mathrm{dr}}^{-1} + \\ 4\rho_{\mathrm{hv}}(Z_{\mathrm{dr}}^{1/2} - Z_{\mathrm{dr}}^{-1/2})\cos(\Phi_{\mathrm{DP}}) \end{array}\right] \quad (22)$$

Let's assume a Gaussian shape for the copolar lobe and the following offset Gaussian shape

$$|F_{\mathrm{hv}}(\theta,\phi)|^2 = g_{\mathrm{hv}}\,|f_{\mathrm{hv}}(\theta,\phi)|^2 = g_{\mathrm{hv}}\exp\left[-\frac{(\theta-\theta_{\mathrm{p}})^2+(\phi-\phi_{\mathrm{p}})^2}{4\sigma_{\mathrm{hv}}^2}\right],$$

for each of the cross-polar lobes. Here θ_{p} and ϕ_{p} are angular locations of the cross-polar radiation peaks. Then define

$$W_4 = \frac{\int F_{\mathrm{hh}}^2 \,|F_{\mathrm{hv}}|^2 d\Omega}{\int F_{\mathrm{hh}}^4 d\Omega} = 4\frac{2g_{\mathrm{hv}}\theta_{1\mathrm{x}}^2}{g_{\mathrm{hh}}(\theta_{1\mathrm{x}}^2+\theta_{\mathrm{l}}^2)} e^{-\frac{4\theta_{\mathrm{p}}^2\ln(2)}{(\theta_{\mathrm{l}}^2+\theta_{1\mathrm{x}}^2)}}, \quad (23)$$

as the antenna's bias weighting factor for a 4-lobed cross-polar radiation pattern. The 3 dB width of the one-way copolar power pattern is θ_1, whereas the 3 dB one-way width of each cross-polar lobe is θ_{1x}. Fradin's equations (Appendix) are used to compute the location of the cross-polar peaks for a center-fed parabolic reflector. For example, the WSR-88D reflector illuminated with radiation at a wavelength of 5 cm, shows θ_{p} measured (i.e., about 0.5°; Fig. 5) agrees with θ_{p} calculated (i.e., 0.47°) from (A.3).

For rain Z_{dr}> 1, and from (22) it is deduced the largest bias is negative if Φ_{DP} = 0°. Under this condition (i.e., Φ_{DP} = 0°) and for ρ_{hv} = 1, δZ_{DR} normalized with W_4 is plotted in Fig. 4. Note that the maximum negative bias grows almost linearly with differential reflectivity (i.e., $\delta Z_{\mathrm{DR}} / W_4 \approx$ -6.15 Z_{DR}) in the range of 0 to 3 dB. Let's now examine a specific polarimetric weather radar example.

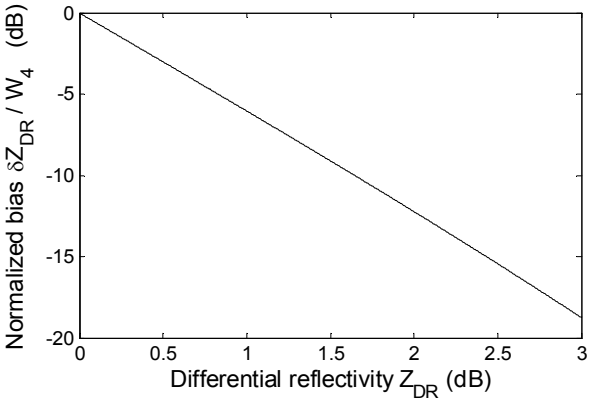

Fig. 4 Maximum normalized bias (i.e., a negative bias) versus Z_{DR} for an antenna having a cross-polar radiation pattern dominated by four cross-polar lobes which are equally spaced on a circle θ_p from the copolar axis.

Cross-polar pattern measurements (Fig. 5) indicate $\theta_{1\mathrm{x}} \approx \theta_{\mathrm{l}}$ (i.e., 0.42° for the University of Oklahoma's polarimetric radar called OU PRIME, and 0.93° for the 10-cm wavelength KOUN), and $\theta_{\mathrm{p}} \approx \theta_{\mathrm{l}}$ as also suggested by theory (A.3). Assume the ratio of gains ($g_{\mathrm{hv}}/g_{\mathrm{hh}}$) = 0.001 (-30 dB which is an upper value; Fig.5 suggests -35 dB). Then W_4 in (23) equals $g_{\mathrm{hv}}/g_{\mathrm{hh}}$ and the maximum negative bias (i.e., at Φ_{DP} = 0°) obtained from Fig. 4 is about -0.0062 Z_{DR} (dB), a negligible amount.

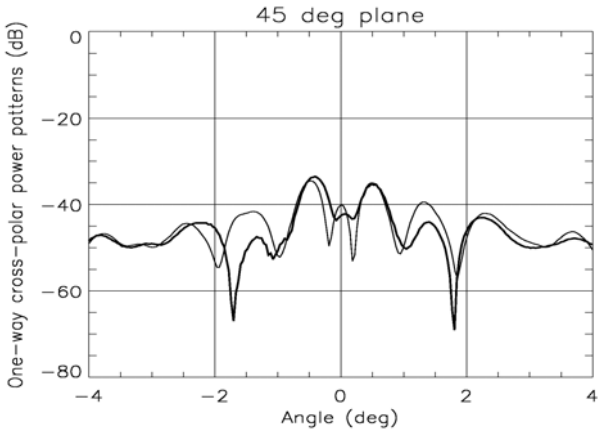

Fig. 5 Cross-polar radiation pattern functions $|F_{\mathrm{hv}}(\theta)|^2 / F_{hh}^4(0)$ (thick), and $|F_{\mathrm{vh}}(\theta)|^2 / F_{hh}^4(0)$ (thin line) along the 45° diagonal of the OU PRIME antenna illuminated with radiation at a wavelength of 5.333 cm.

The primary reason for the significantly better performance of this type of cross-polar radiation pattern is that the four symmetrically located pattern peaks alternate sign so that there is cancellation of some cross-polar contribution. Another reason is the bias weighting factor is proportional to the integral of the square of the normalized cross-polar radiation, whereas it is proportional to the normalized radiation if the cross-polar pattern is coaxial with the copolar pattern. Furthermore, the displacement of these peaks from the copolar beam axis causes the cross product of copolar pattern with the cross-polar pattern to be smaller than in case where the cross-polar main lobe is coaxial with the copolar beam.

3.4.1 AN EXAMPLE

In Fig. 5 are two cross-polar patterns measured for the OU PRIME radar. This antenna reflector is a replica of the WSR-88D reflector, but has four feed-support struts as opposed to three, and is illuminated with 5 cm wavelength radiation. Thus the beam width is 0.44°, i.e., about half the beamwidth of the WSR-88D radar.

This type of cross polar radiation pattern can be represented as sum of a centered pattern (Fig. 2a) with the quad pattern (Fig. 2b). The exact computation of the bias is straight-forward, although tedious. Significant simplification is possible by noting that the dominant factor is the first order (in powers of F_{hv}) term $\int F_{hh}^3 |F_{hv}| d\Omega$ for a coaxial cross-polar peak, and the second order term, $\int F_{hh}^2 |F_{vh}|^2 d\Omega$ for off-set cross-polar peaks.

The two-way copolar power pattern and the two normalized cross products (i.e., $F_{hh}^3 |F_{hv}|$ and $F_{hh}^2 |F_{vh}|^2$) in the three principal planes are in Figs. 6a, 6b, 6c. It is clear from Fig. 6 that the cross-polar pattern peak collocated with copolar beam axis contributes most to the bias. Because the normalized term $F_{hh}^3 |F_{vh}| / F_{hh}^4(0)$ has almost the same angular width as F_{hh}^4 (Fig. 6a), the antenna's bias weighting factor, W_{vh} (17b) can be approximated with $\sqrt{g_{vh} / g_{hh}}$ (0.01 in this case). Furthermore if $|F_{hv}| = |F_{vh}|$, $W_{hv} = W_{vh} = W = 0.01$. With this value the maximum positive bias (i.e., if γ_{hv} = 90°, and β = – 90°) can be read from the top curve in Fig. 3. It is about 0.35 dB. This is significant but unlikely to happen as it requires a juxtaposition of γ = 90°, β = -90, and $\Phi_{DP} = 0^o$.

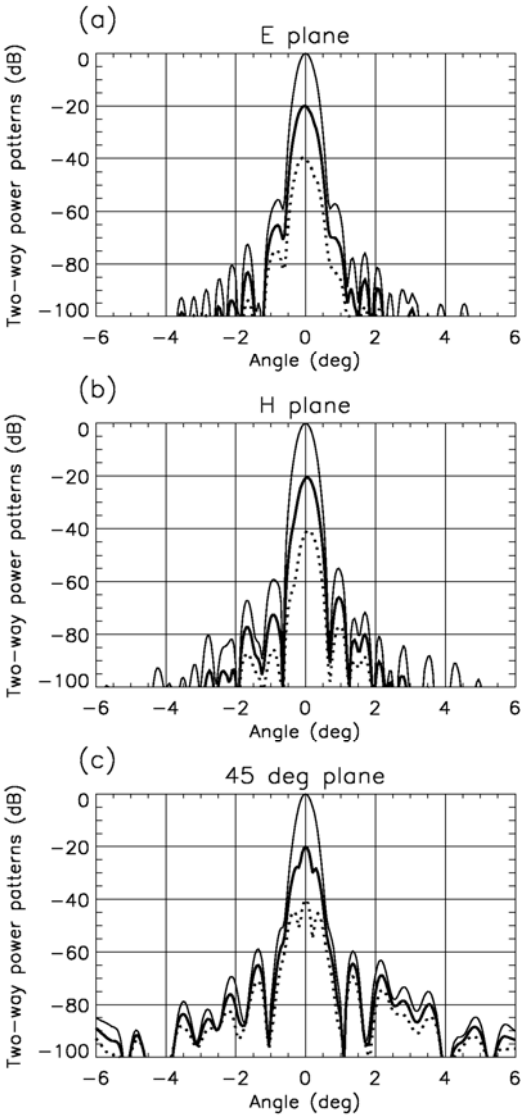

Fig. 6 a) The two-way pattern $f_{hh}^4(\theta)$ (i.e., the solid thin curve), the normalized product $F_{hh}^3 |F_{vh}| / F_{hh}^4(0)$ (i.e., the solid thick curve), and the normalized product $F_{hh}^2 |F_{vh}|^2 / F_{hh}^4(0)$ (i.e., the dotted curve) in the E plane. b) Same as in a) except measurements are made in the H plane. c) Same as in a) but in the 45° plane.

The maximum negative bias contributed by the four cross-polar peaks is computed using equations (22) and (23) and using, from Fig.5, the ratio (g_{hv}/g_{hh}) ≈ 3.16 10^{-4} (i.e., about -35 dB), and

$\theta_p = \theta_{1x} = \theta_1$. Thus the maximum negative bias is about -0.002 Z_{DR}, which is insignificant (positive biases are smaller yet).

4. Alternate Transmit and Simultaneous Receive (AHV) mode

Next consider the AHV mode and apply the same formalism starting with (3). For computing P_h set the lower element in the right most matrix to zero, and for P_v set the upper element to zero. Then, after performing the multiplications, it can be shown all first and many second order terms in F_{hv} and F_{vh} vanish; thus the powers can be expressed as

$$\frac{P_h}{<|s_{vv}|^2>} \sim Z_{dr}\int F_{hh}^4 d\Omega + 2\rho_{hv}\sqrt{Z_{dr}} \times \cos(\Phi_{DP} + 2\gamma_{vh})\int F_{hh}^2 |F_{vh}^2| d\Omega \quad , \quad (25a)$$

$$\frac{P_v}{<|s_{vv}|^2>} \sim \int F_{hh}^4 d\Omega + 2\rho_{hv}\sqrt{Z_{dr}} \times \cos(\Phi_{DP} - 2\gamma_{hv})\int F_{hh}^2 |F_{hv}^2| d\Omega \quad . \quad (25b)$$

Thus bias, $\delta Z_{DR}^{(A)}$, for the AHV mode is

$$\delta Z_{DR}^{(A)} \approx 20\log(e)\rho_{hv} \times \begin{Bmatrix} W_{vh}^{(A)} Z_{dr}^{-1/2}\cos(\Phi_{DP} + 2\gamma_{vh}) \\ -W_{hv}^{(A)} Z_{dr}^{1/2}\cos(\Phi_{DP} - 2\gamma_{hv}) \end{Bmatrix} \text{ (dB)} \quad , \quad (26)$$

where

$$W_{vh}^{(A)} = \frac{\int F_{hh}^2 |F_{vh}|^2 \, d\Omega}{\int F_{hh}^4 d\Omega} , \quad (27a)$$

$$W_{hv}^{(A)} = \frac{\int F_{hh}^2 |F_{hv}|^2 \, d\Omega}{\int F_{hh}^4 d\Omega} . \quad (27b)$$

If slant linear polarization is transmitted for the SHV mode and $F_{hv} = F_{vh}$, (15) is identical in form to (26). Comparing (27a, b) with (14a, b) it is evident that, for cross-polar radiation patterns having a prominent peak on-axis with the copolar peak, the bias factors W for the AHV mode are significantly smaller than for the SHV mode, and thus Z_{DR} bias for the AHV mode is substantially reduced.

The radiation patterns seen in Fig. 5 suggest the on-axis cross-polar radiation is well below the copolar peak (i.e., -40 dB lower) whereas the cross-polar peak measured on a WSR-88D antenna is about -32 dB (Doviak and Zrnic, 1998, Figs. II.9). Note that both these measurements were made at the same manufacturer's site. It is likely that the smaller copolar beamwidth of the 5 cm OU PRIME mitigates reflection from the terrain that could have contributed to the on-axis cross-polar radiation peak. It should also be noted for an antenna of similar design, Bringi and Chandrasekar (2001, Fig. 6.15) report principal plane cross-polar radiation, measured at another manufacturer's test range, is everywhere below -45dB.

Thus, let's assume that we have a center-fed antenna in which the on-axis radiation lobe is negligible. Under this condition let's compare the Z_{DR} biases using the SHV and AHV modes. Thus, assuming four equal cross-polar lobes offset from the beam axis, we use (22) and (26) for this comparison. In this case the antenna's bias factor W_4 is the same for both modes. For rain it is safe to set $\rho_{hv} \approx 1$, and note $Z_{dr} \geq 1$. Thus we can write $Z_{dr} = 1 + \Delta$, and assume that $\Delta < 1$. Under these conditions it can be shown that (22) reduces to

$$\frac{\delta Z_{DR}^{(S)}}{W_4} = -20(Z_{dr} - 1)\log(e)[1 + 2\cos\Phi_{DP}] \quad (28a)$$

which is the normalized bias for the SHV mode, whereas for the AHV mode, (26) becomes

$$\frac{\delta Z_{DR}^{(A)}}{W_4} = -20(Z_{dr} - 1)\log(e)\cos\Phi_{DP} . \quad (28b)$$

Comparing these two, the SHV Z_{DR} bias is about 3 times larger than that for the AHV mode. Nevertheless, assuming that $W_4 \leq 3.16\ 10^{-4}$ (i.e., F_{hv} peak at least -35 dB below the copolar peak; Fig. 5), SHV bias is approximately 0.002 Z_{DR}, which is still insignificant.

5. SUMMARY AND CONCLUSIONS

Herein we investigate the affects differential reflectivity bias δZ_{DR} has on rainfall measurements (section 2). δZ_{DR} depends on several parameters including cross-polar radiation as well as differential reflectivity Z_{DR} itself. For accurate rainfall measurement δZ_{DR} should be smaller than about 10% of Z_{DR} (in dB, Fig. 1).

With this in mind we set out to quantify the bias caused by cross-polar radiation. We examine two types of cross-polar patterns commonly observed. One has a cross-polar main lobe centered on the copolar main lobe, the other has four lobes of equal magnitude and displaced symmetrically about the beam axis. Use of customary approximations (i.e., radiation lobes having Gaussian shape), and uniformly distributed scatterers with vertical axes of symmetry, leads to simple analytic equations for the antenna's differential reflectivity's bias weighting factors W_{hv} and W_{vh} (i.e., the spatial integral of the normalized products of copolar and cross-polar radiation patterns).

Antennas having multiple cross-polar lobes associated with the reflector, but cross-polar nulls along the principal planes, cause significantly less bias than those having a single cross-polar lobe centered on the copolar beam axis. This latter situation appears to be an artifact that causes unacceptable bias if the transmitted wave is circularly polarized and the copolar and cross-polar voltage patterns are 90° out of phase (Fig. 3, top curve); this bias can be reduced by about a factor of two (on a dB scale) if the transmitted wave is slant linear at $\pm 45^{o}$ (Fig. 3, middle curve). Then, if these coaxial lobes have the same widths, the level of cross polar peak radiation must be at least 45 dB below the copolar peak to keep the Z_{DR} bias under 0.1 dB. This stringent condition can be relaxed to 32 dB if the copolar and cross-polar voltage patterns are in or out of phase with each other, and $Z_{DR} \le 2$ dB (Fig. 3, bottom curve). But recent data for research weather radars (e.g. Fig.5 herein, and Fig.6.15 of Bringi and Chandrasekar, 2001), as well as that for the polarimetric prototype WSR-88D antenna, (Baron, 2009) indicate on-axis cross-polar gain can be 40 or more dB below the copolar gain.

It is suggested that the on-axis cross-polar radiation observed for large antennas is likely due to reflection from surrounding terrain, and not an inherent characteristic of the antenna. If the cross-polar radiation has an on-axis null, the only significant cross-polar radiation peaks are the four equal-gain lobes due to the reflector (section 3d); the gain of these lobes needs to be below -21 dB to insure that Z_{DR} bias is less than 0.1 dB (at $Z_{DR} \le$ 2 dB). Measurements (Fig. 5) suggest these gains are well below -30 dB.

In agreement with previous investigations, it turns out that Z_{DR} bias is not an issue for polarimetric radars utilizing the alternate (AHV) mode. For the simultaneous (SHV) mode, bias in Z_{DR} is larger, but it can be controlled with appropriate antenna design (i.e., minimizing the on-axis cross-polar radiation) so that its effect on rain rate errors is negligible (section 4).

6. *Acknowledgments*

Pattern measurements of the OU PRIME antenna were provided by Enterprise Electronics Corporation and Dr. Boon Leng Cheong of the Atmospheric Radar Research Center at the University of Oklahoma. Funding for CIMMS authors came from NOAA/Office of Oceanic and Atmospheric Research under NOAA-University of Oklahoma Cooperative Agreement NA17RJ1227, U.S. Department of Commerce.

7. APPENDIX

Cross-polar radiation induced by the parabolic reflector

Fradin (1961, Section 7.2) shows that the copolar and cross-polar fields in the aperture of a center-fed parabolic reflector illuminated with the field of a vertical (i.e., y directed) dipole are given by

$$E_y = -A\frac{4f^2 + \rho^2\cos 2\varphi}{(4f^2 + \rho^2)^2}\ , \qquad \text{(A1)}$$

and

$$E_x = -A\frac{\rho^2 \sin 2\varphi}{(4f^2 + \rho^2)^2}\ , \qquad \text{(A2)}$$

where the horizontal x direction and y are in the aperture of the parabolic reflector, f is its focal length (for the WSR-88D, f =0.375 D; D is the antenna diameter), A is a complex constant (dependent on f, D, the dipole moment, and wavelength), $\rho = \sqrt{x^2 + y^2}$ is the radial distance from the z axis to any point in the aperture plane, and φ is the angle measured from the x axis.

Using these equations, it is easily seen that the cross-polar field has nulls along the principal axes (i.e., x and y), and each quarter sector of the aperture is a source of cross-polar radiation having alternating phases. Thus the far field pattern should have, in absence of spar and feed blockage and reflector surface perturbations, nulls along the principal planes. Furthermore, for the WSR-88D antenna, (A2) shows the peak of the aperture's cross-polar field is on the periphery of the aperture and along diagonals at $\pm 45^{o}$. We shall treat each sector as a source of radiation emanating from a phase center located at the center of gravity of the cross-polar aperture function (i.e., A2) in each sector. Because the aperture distribution in each sector is symmetrical about the φ = 45° diagonals, the four phase centers lie along these diagonals. Using (A2) we compute the phase centers to be at the radial distance ρ_c = 0.71 D/2.

The cross-polar radiation has a peak at an angle θ_p, measured from the copolar beam axis (i.e., z axis), where radiation from each of the four sectors constructively add. The sectors either side of the diagonals always add in phase, but the sectors along the diagonal add in phase at

$$\theta_p = \sin^{-1}\left(\frac{\lambda}{2\rho_c}\right). \qquad \text{(A3)}$$

For the KOUN parameters, λ = 0.11 m and D = 8.53 m, and thus θ_p computes to be 1.04°. We conclude there are four principal lobes of cross-polar radiation, one each along the azimuthal directions $\varphi = \pm 45^{o}$, and $\varphi = \pm 135^{o}$, and at an angular displacement given by (A3). Such large cross-polar radiation lobes are suggested in the pattern measurements presented by Bringi and Chandrasekar (2001, Fig. 6.15), as well as in the pattern data presented in Fig.5.

8. *REFERENCES*

Balakrishnan, N., D. S. Zrnic, J. Goldhirsh, and J. Rowland, 1989: Comparison of simulated rain rates from disdrometer data employing polarimetric radar algorithms. *J. Atmos. Oceanic Technol.*, **6**, 476-486.

Baron Services, Inc., 2009: "WSR-88D Dual-Polarization Program, Report: Antenna Component Test", Baron Services, Inc. 4930 Research Park Drive, Huntsville, AL, 35805, 116 pp.

Brandes, E., G. Zhang, and J. Vivekanandan, 2002: Experiments in rainfall estimation with a polarimetric radar in a subtropical environment, *J. Atmos. Meteor.*, **41**, pp. 674-685.

Bringi, V. N., and V. Chandrasekar, 2001: "Polarimetric Doppler Weather Radar". *Cambridge University Press*, Cambridge UK, 636 pp.

Chandrasekar, V., and R. J. Keeler, 1993: Antenna pattern analysis and measurements for multiparameter radars. *J. Atmos. Oceanic Technol.,***10,** 674-683.

Doviak, R.J., and D. S. Zrnic, 2006: "Doppler radar and weather observations". Second edition, reprinted by *Dover*, Mineola, NY 562 pp.

Doviak, R. J., V. Bringi, A. Ryzhkov, A. Zahrai, and D. Zrnic, 2000: Considerations for polarimetric upgrades to operational WSR-88D radars. *J. Atmos. Oceanic Technol.,***17,** 257-278.

Doviak, R. J., and D. Zrnic, 1998: Polarimetric upgrades to improve rainfall measurements. NOAA/NSSL technical report (WEB site: http://publications.nssl.noaa.gov/wsr88d_reports/2pol_upgrades.pdf) 110 pp.

Durić, A., A. Magun, A. Murk, C. Mätzler, and N. Kämpfer, 2008: The Fully Polarimetric Imaging Radiometer SPIRA at 91 GHz. *IEEE Trans. Geosci. Remote Sens.*, **46**, 2323-2336.

Fradin, A. Z., 1961: "Microwave antennas". *Pergamon Press*, London, UK, pp. 668.

Hubbert, J. C., M. Dixon, S. Ellis, and G. Meymaris, 2009: Simultaneous vertical and horizontal transmit radar data and polarization errors. 25th Conference on Interactive Information and Processing Systems (IIPS) for Meteorology, Oceanography, and Hydrology. Paper 15.4. AMS, Phoenix AZ.

Matrosov, S. Y., K. A. Clark, B. E. Martner, and A. Tokay, 2002: X-Band Polarimetric Radar Measurements of Rainfall. *J. Appl. Meteor.*, **41**, 941–952

Paramax Systems Corp., 1992: Test report CDRL 246; Antenna pedestal, Part 1 of 4, Document

#TR1218305, 1 July. Prepared by Paramax Systems Corp. for the U. S. Department of Commerce, Office of Procurement, Washington, DC 20230.

Potter, P. D., 1963: A new horn antenna with suppressed sidelobes and equal beamwidths. *Microwave Journal*, 71-78.

Ryzhkov, A. V., S. E. Giangrande, V. M. Melnikov, and T. J. Schuur, 2005a: Calibration issues of dual-polarization radar measurements. *J. Atmos. Oceanic, Technol.,* **22,** 1138-1155.

Ryzhkov, A. V., T. J. Schuur, D. W. Burgess, P. L. Heinselman, S. E. Giangrande, and D. S. Zrnic, 2005b: The Joint Polarization Experiment: Polarimetric rainfall measurements and hydrometeor classification. *Bull. American Met. Soc.,* **86**, 809-824.

Ryzhkov, A. V., and D. S. Zrnic, 1995: Comparison of dual-polarization radar estimators of rain. *J. Appl. Meteor.,* **12**, 249-256.

Sachidananda, M., and D. S. Zrnic, 1985: Z_{DR} measurement considerations for a fast scan capability radar. *Radio Sci.,* **20**, 907-922.

Wang, Y., V. Chandrasekar, and V. N. Bringi, 2006: Characterization and evaluation of hybrid polarization observation of precipitation. *J. Atmos. Oceanic Technol.*, **23,** 552-572.

Wang, Y., and V. Chandrasekar, 2006: Polarization isolation requirements for linear dual-polarization weather radar in simultaneous transmission mode of operation. *IEEE Trans. Geosci. Remote Sens.,* **44,** 2019-2028.

Zhang, G., J. Vivekanandan, and E. Brandes, 2001: A method for estimating rain rate and drop size distribution from polarimetric radar measurements. *IEEE Trans. Geosci. Remote Sens.,* **39**, 830-841.

Zrnic, D. S., A. Ryzhkov, J. Straka, Y. Liu, and J. Vivekanandan, 2001: Testing a procedure for automatic classification of hydrometeor types. *J. Atmos. Oceanic Technol.,* **18,** 892-913.

Zrnic, D. S., V. M. Melnikov, and J. K. Carter, 2006: Calibrating differential reflectivity on the WSR-88D. *J. Atmos. Oceanic Technol.,* **23,** 944-951.